PAPER

# Impact of local chemical ordering on deformation mechanisms in single-crystalline CuNiCoFe high-entropy alloys: a molecular dynamics study

IOP Publishing Modelling and Simulation in Materials Science and Engineering

Modelling Simul. Mater. Sci. Eng. **31** (2023) 085014 (13pp) https://doi.org/10.1088/1361-651X/ad04f3

# Impact of local chemical ordering on deformation mechanisms in single-crystalline CuNiCoFe high-entropy alloys: a molecular dynamics study

**Siyao Shuang[1], Yanxiang Liang[2], Xie Zhang[3], Fupin Yuan[4], Guozheng Kang[1] and Xu Zhang[1,*]**

[1] Applied Mechanics and Structure Safety Key Laboratory of Sichuan Province, School of Mechanics and Aerospace Engineering, Southwest Jiaotong University, Chengdu 610031, People's Republic of China
[2] Institute of Systems Engineering, China Academy of Engineering Physics (CAEP), Mianyang 621999, People's Republic of China
[3] School of Materials Science and Engineering, Northwestern Polytechnical University, Xi'an 710072, People's Republic of China
[4] State Key Laboratory of Nonlinear Mechanics, Chinese Academy of Science, Institute of Mechanics, Beijing, People's Republic of China

E-mail: xzhang@swjtu.edu.cn

Received 7 August 2023; revised 7 October 2023
Accepted for publication 19 October 2023
Published 31 October 2023

**Abstract**

High-entropy alloys (HEAs), composed of multiple constituent elements with concentrations ranging from 5% to 35%, have been considered ideal solid solution of multi-principal elements. However, recent experimental and computational studies have demonstrated that complex enthalpic interactions among constituents lead to a wide variety of local chemical ordering (LCO) at lower temperatures. HEAs containing Cu typically decompose by forming of Cu-rich phases during annealing, thus affecting mechanical properties. In this study, CuNiCoFe HEA was chosen as a model with a tendency for Cu segregation at low temperatures. The formation of LCO and its impact on the deformation behaviors in the single-crystalline CuNiCoFe HEA were studied via molecular dynamics simulations. Our results demonstrate that CuNiCoFe HEA decomposes by Cu clustering, in agreement with prior experimental and computational studies, owing to insufficient configuration entropy to compete against the mixing enthalpy at lower temperatures. A softening in ultimate stress in the LCO models was observed compared to the random solid solution models. The

* Author to whom any correspondence should be addressed.

softening is due to the lower unstable stacking fault energy, which determines the nucleation event of dislocations, thereby rationalizing the dislocation nucleation in the Cu-rich regions and the softening of the overall ultimate strength in the LCO models. Additionally, the inhomogeneous FCC–BCC transformation is closely associated with concentration inhomogeneity. CuNiCoFe HEA with LCO can be regarded as composites, consisting of clusters with different properties. Consequently, concentration inhomogeneity induced by LCO profoundly impacts the mechanical properties and deformation behaviors of the HEA. This study provides insights into the effect of LCO on the mechanical properties of CuNiCoFe HEAs, which is crucial for developing HEAs with tailored properties for specific applications.

Supplementary material for this article is available online

Keywords: high-entropy alloy, local chemical order, concentration inhomogeneity, softening effect, plasticity

(Some figures may appear in colour only in the online journal)

## 1. Introduction

Multi-principal element alloys, often referred to as high-entropy alloys (HEAs), have drawn considerable interest among the scientific and industrial communities owing to their exceptional mechanical properties [1]. HEAs typically contain multiple principal elements with an atomic percentage between 5% and 35% to achieve a high configurational entropy ($S_c$), forming an ideal random solid solution (RSS) alloy. HEAs usually correspond to a configurational entropy higher than 1.61 $R$ estimated from $S_c = -R\sum_{i=1}^{N} x_i \ln(x_i)$, where $R$ is the gas constant and $x_i$ is the molar fraction of the $i$th element. However, the ideal solid solution state may only exist at very high temperatures where entropy dominates the free energy. As temperature decreases, the contribution of the configurational entropy becomes insufficient to compete against the mixing enthalpy, leading to varying degrees of local chemical ordering (LCO). Real-world HEAs are often processed and utilized at relatively low temperatures, where enthalpic interactions dominate the change of Gibbs free energy. For example, the pioneering Cantor alloy, which is considered an RSS alloy, decomposes after annealing below 900 °C [2]. Recently, Zhang *et al* [3] observed LCO in the equiatomic CrCoNi medium-entropy alloy (MEA) using energy-filtered transmission electron microscopy. They observed a 25% increase in yield strength related to the strengthening effect of LCO. In addition, local segregation and LCO have been found in several MEAs and HEAs [4–18], indicating that enthalpic interactions play a critical role in multi-principal alloys.

Computational simulations have been increasingly popular to study atomic segregation due to the challenging experimental techniques involved. Chen *et al* [18] studied the LCO in CoCuFeNiX (X = Pd or Ti) HEAs using hybrid Monte Carlo (MC) molecular dynamics (MD) methods. They proposed that chemical-affinity disparity and exclusivity promote the formation of various microstructures, including decomposition, short-range ordering, and cluster formation. Guo *et al* [16] investigated the effect of LCO on mechanical properties in the Cantor alloy. Li *et al* [9] studied the trapping effect of LCO on dislocation mobility in the CoNiCr MEA. As a result, CoCr clusters were observed to pin dislocation segments, resulting in additional strengthening. Furthermore, Jian *et al* [17] found that Shockley partial (SP) dislocations preferentially nucleate in the CoCr clusters, which have the lowest unstable stacking

fault energy (SFE) in the CoNiCr MEA. Besides, the temperature-related atomic segregation also affects the stability of grain boundaries [19], and radiation resistance [14]. Therefore, it is critical to investigate the underlying mechanisms concerning LCO and its impact on deformation behaviors.

Most HEAs containing Cu element usually decompose by forming Cu-rich phase [20–22]. Grain boundary segregation of Cu element can decrease the grain size in FeNiCrCoCu HEA and decrease wear rate [21]. Besides, the Cu-rich phase in FeNiCrCoCu HEA can also lead to a decrease in hardness [22]. The impact of Cu segregation on mechanical properties is highly complex. In this study, CuNiCoFe HEA was chosen as a model with a tendency for Cu segregation at low temperatures. LCO and its impact on deformation mechanisms in the equiatomic single-crystalline CuNiCoFe HEA were investigated. The hybrid MC/MD method was used to prepare structural models stabilized by configurational entropy at different temperatures. The results indicate that the CuNiCoFe HEA exhibits RSS states at elevated temperatures, but decomposes at lower temperatures by Cu precipitation. Models with varying degrees of chemical ordering were then subjected to a uniaxial tensile test to study the impact on mechanical performance and deformation behaviors. Additionally, the origin of Cu clusters and the profound impact of LCO on deformation behaviors were emphasized.

## 2. Models and methods

The simulation cell in this study consisted of 1372 000 atoms with $x$-[100], $y$-[010] and $z$-[001] crystal orientations. The dimensions of the cell were 25 nm $\times$ 25 nm $\times$ 25 nm. The atomic interactions in CuNiCoFe HEA were described using an embedded atom method potential developed by Zhou *et al* [23], which has been extensively benchmarked and successfully applied in previous atomistic simulations [14, 19]. The reliability was further confirmed against reference data in prior studies [14]. To generate LCO models, the hybrid MC/MD method [9, 12, 18, 24] in the variance-constrained semi-grand-canonical ensemble [25], as implemented in the Large-scale Atomic/Molecular Massively Parallel Simulator code [26], was employed. Before simulation, three initial RSS samples were annealed using the MC/MD method at 300, 400, and 500 K for 1000 ps until the potential energy converged to obtain the thermodynamically stable configurations. For every 20 MD simulation steps, there was an MC step with a $\kappa$ parameter of $10^3$ [27], which constrains the variance. The models were then cooled down to 0 K under the isobaric-isothermal (NPT) ensemble. An energy minimization process was carried out on the models to optimize the configurations until the total energy converges within $10^{-15}$ eV. Finally, the annealed models along with the RSS model were subjected to uniaxial tension at 300 K with a strain rate of $5 \times 10^8$ s$^{-1}$, while the pressure in the other two directions was kept at zero. The simulation results were visualized using the common neighbor analysis (CNA) [28] and dislocation extraction algorithm [29], as implemented in OVITO [30]. To quantify the degree of LCO, the pairwise multicomponent LCO parameter [9] was adopted, defined as $\alpha_{ij}^m = \left(p_{ij}^m - C_j\right) / \left(\delta_{ij} - C_j\right)$. In the formula, $m$ represents the $m$th nearest-neighbor shell of the central atom $i$, $p_{ij}^m$ denotes the average probability of finding a $j$-type atom around the $i$-type atom in the $m$th shell, $C_j$ is the average fraction of $j$-type atoms in the system, and $\delta_{ij}$ is the Kronecker delta function. A positive $\alpha_{ij}^m$ means the tendency of segregation when the element is the same (i.e. $i = j$), while a negative $\alpha_{ij}^m$ represents the opposite. Conversely, when the elements are different (i.e. $i \neq j$) $\alpha_{ij}^m$ means the opposite. In this study, the LCO parameters were calculated using the first nearest-neighbor ($m = 1$).

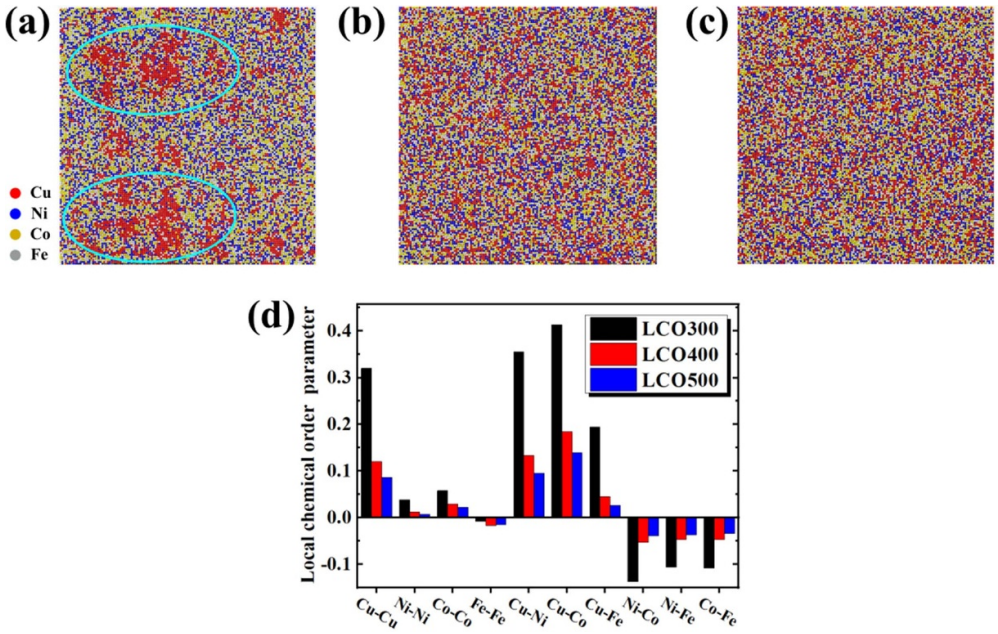


**Figure 1.** Chemical distribution maps of the CuNiCoFe high-entropy alloy (HEA) with local chemical order (LCO) after Monte Carlo (MC)/molecular dynamics (MD) simulations at (a) 300 K, (b) 400 K and (c) 500 K, labeled by LCO300, LCO400, and LCO500, respectively. (d) Pairwise chemical short-range order parameter for different samples.

## 3. Results and discussion

### *3.1. Origin of LCO for CuNiCoFe HEA*

Figures 1(a)–(c) show the LCO models annealed at 300, 400, and 500 K, labeled by LCO300, LCO400, and LCO500, respectively. The variation of the potential per atom during MC/MD simulations is shown in figure S1, which suggests that potential energy decreases with the formation of energetically favorable LCO structures. Note that at such low temperatures, atomic diffusion and chemical ordering are inhibited. Nevertheless, lower temperatures enhance enthalpic interactions and suppress entropic effects, promoting local segregation. The result shows that the CuNiCoFe HEA decompose by small Cu clusters after annealed, especially at 300 K. The LCO drives the formation of Cu-rich and Cu-depleted phase, which has been experimentally observed in CoCrFeMnCu HEAs [31]. As summarized in figure 1(d), all $\alpha$ values deviate from the RSS in either the positive or negative direction, with Cu segregation being the most pronounced. When the annealing temperature decreases from 500 K to 300 K, the value of $\alpha_{\mathrm{Cu\text{-}Cu}}$ increases from 0.086 to 0.32, indicating the Cu segregation tendencies. There is no obvious tendency to form Ni–Ni, Ni–Co or Fe–Fe pairs. Due to Cu segregation, the other three elements avoid Cu, leading to a positive $\alpha$ value of Cu–Ni (0.35), Cu–Co (0.41) and Cu–Fe (0.19), indicating the avoidance of these pairs. Besides, the negative $\alpha$ value of Ni–Co ($-0.13$), Ni–Fe ($-0.1$) and Co–Fe ($-0.1$) suggests slight tendencies of forming these pairs. At lower temperatures, the configuration entropy is insufficient to compete against the mixing enthalpy and local segregation occurs in the HEAs or MEAs. For example, the preference towards V–Co and V–Ni pairs and avoidance of V–V pairs formed in the VCoNi MEA after

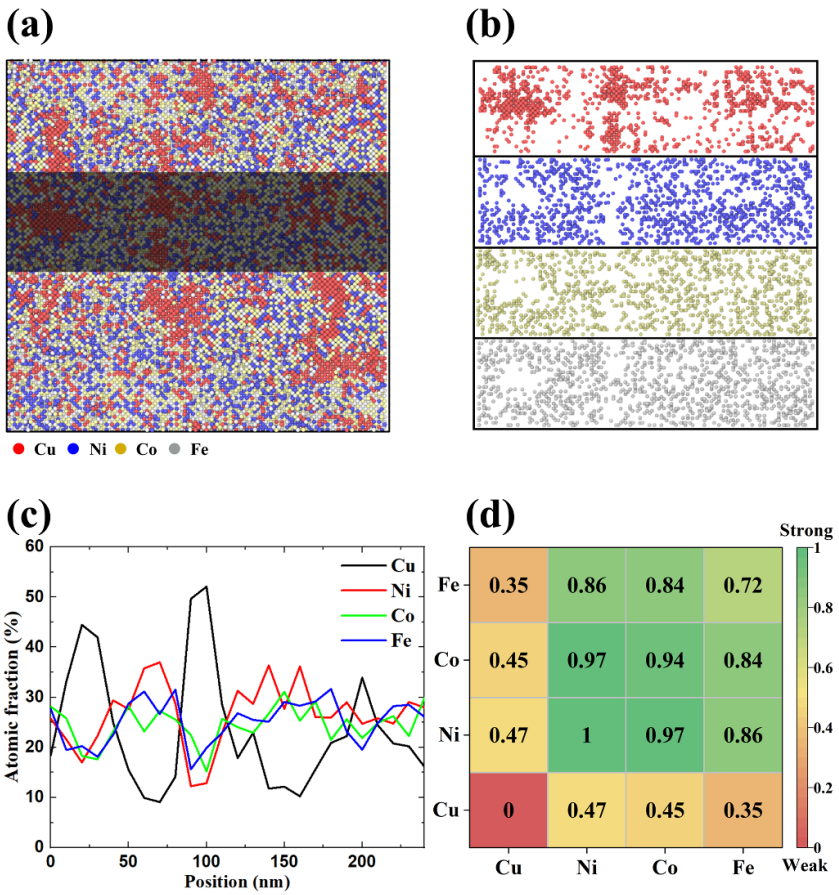


**Figure 2.** (a) Atomic configuration of LCO300. (b) Spatial distribution of constituent element (Cu, Ni, Co and Fe) in the black region in (a). (c) Atomic fraction of the constituent elements in the black region in (a). (d) Normalized chemical affinity of elemental pairs for the CuNiCoFe HEA. The data was taken from Chen *et al* [18] based on the MD simulations. A larger value of chemical affinity indicates the tendency of the pair.

annealed [11]. Moreover, real-world alloys are usually processed or used at relatively low temperatures, where complex enthalpic interactions among various elements drive the formation of LCO or grain boundary segregations [2, 24, 31–33].

To further understand the LCO in the CuNiCoFe HEA, detailed analyses of the spatial arrangement of constituent elements were conducted. Figure 2(b) shows the distribution map of constituents in the black region of figure 2(a) taken from LCO300. The result demonstrates that the RSS CuNiCoFe HEA decomposes to form some local Cu clusters. Cu segregates in the left region (0 to ∼50 nm and ∼90 to ∼110 nm), as shown in figure 2(c). In the other regions, Ni, Co and Fe atoms are randomly mixed. These results correspond well to the discussion concerning LCO parameters in figure 1(d).

In order to probe the origin of LCO in CuNiCoFe HEA, the chemical affinity of elemental pairs in CuNiCoFe HEA is further analyzed. The data is taken from a previous study by Chen *et al* [18] based on MD computations. The cohesive energies of elemental pairs in the alloy were compared and normalized as the judgement of chemical affinity. As shown in figure 2(d),

the chemical affinity of Cu–Cu (0) is the weakest, inconsistent with the tendency of Cu segregation in figures 1 and 2. Besides, the chemical affinities of pairs related to Cu (Cu–Ni, Cu–Co and Cu–Fe) are weaker than other pairs. In contrast, the chemical affinities of Ni–Ni (1.00), Ni–Co (0.97) and Co–Co (0.94) are much stronger. From the chemical-affinity relationship among elementary pairs, we can know that the low- and medium-energy clusters (such as Ni–Ni, Ni–Co and Co–Co) tend to form during annealing. However, the chemical-affinity disparities among these low-energy pairs are not obvious, hence leading to the formation of NiCoFe RSS. Moreover, the Cu element is excluded by other elements, hence Cu atoms must bond with themselves to form the Cu clusters. Accordingly, the chemical affinity disparity and exclusivity drive atomic segregation and chemical ordering in HEAs. In addition, note that the Cu clusters are loose as shown in figure 2(a), since the formation of high-energy Cu clusters is due to chemical exclusivity rather than active bonding. Recently, Rahul *et al* [20] studied the stability of solid solution phase in the $CoCuFeNiTa_{0.5}$ HEA. The negative enthalpy of mixing of Fe, Co and Ni promotes the formation of solid solution while the positive enthalpy of mixing of Cu drives phase decomposition. Particularly, the EDS mapping [20] suggests the formation of Cu-rich phase in $CoCuFeNiTa_{0.5}$ HEA, which confirmed the simulation results in our study. In addition, the formation of Cu clusters has been observed in various HEAs, such as CoCuFeMnNi HEAs [34–36].

### 3.2. Mechanical properties and deformation behaviors

To explore the impact of LCO on deformation mechanisms in the CuNiCoFe HEA, uniaxial tensile simulations were conducted for both LCO and RSS models. As shown in figure 3(a), there is a linear relationship between strain and stress up to the strain of 0.6 for all samples, indicating that the elastic modulus is not affected by the presence of LCO. However, the ultimate stress decreases due to the existence of LCO, especially for LCO300 as shown in figure 3(a). The RSS model exhibits the highest ultimate strength (3.53 GPa), while the ultimate stress drops with decreasing annealing temperatures in LCO models. Hence, Cu segregation leads to softening in ultimate strength in the CuNiCoFe HEA. To eliminate the influence of randomness, repetitive simulations were also conducted, which suggested that the response of mechanical properties is closely related to LCO. Moreover, it was found that the relationship between the ultimate stress and the LCO parameter $\alpha_{\mathrm{Cu\text{-}Cu}}$ can be described by a linear equation:

$$\sigma_{\mathrm{ultimate}} = A\alpha_{\mathrm{Cu\text{-}Cu}} + B. \tag{1}$$

By fitting the data, the parameters A and B were determined to be $-1.32$ and 3.57, respectively. These results indicate a negative correlation between the strength and LCO in the CuNiCoFe HEA, as shown in figure S3 in the supplementary material. This establishes the certain mathematical relationship between mechanical properties and LCO parameters in HEAs [4], which provides a basis for other computational methods, such as crystal plasticity.

To quantify the deformation behaviors, a planar defect analysis (PDA) algorithm [29] was developed to distinguish various planar defects. The snapshots in figures 3(c) and (d) illustrate the microstructures after tension. Stacking faults (SFs), twin boundaries (TBs) and hexagonal close-packed (HCP) phases were observed during deformation. As shown in figure 3(b), after tension, the volume fraction of the HCP phase in the RSS sample is higher than the other microstructures, indicating that the phase transformation from face-centered cubic (FCC) to HCP dominates the deformation behaviors. However, in LCO models, the nucleation of intrinsic stacking faults, extrinsic stacking faults and TBs dominates the main plastic behavior. With annealing temperature increases, the volume fraction of the HCP phase increases. Overall,

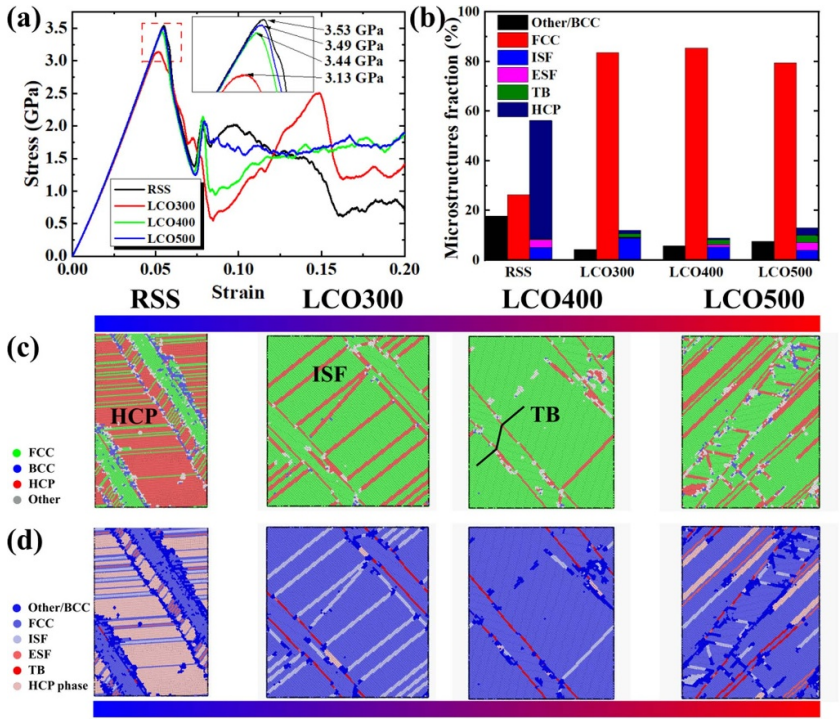


**Figure 3.** (a) Stress–strain curves of the random solid solution (RSS) and LCO models under uniaxial tension. (b) Analysis of the local crystal structures based on planar defect analysis (PDA) algorithm after the tension. (c) Snapshots of crystal structures after tension for all the samples analyzed using CNA. (d) Crystal defect structures analyzed using PDA which quantifies the fraction of crystal defects.

the result indicate that concentration inhomogeneity leads to a transformation of deformation mechanisms. Previous studies [37] have demonstrated that the FCC-HCP martensitic transformation results in a local chemical change and LCO breaking. This process requires additional work to overcome the energy barrier due to the change of alteration of the local chemical environments, which was confirmed by the experimental observation of nanotwins and very thin HCP phase in deformed HEAs [38, 39]. Recent experimental and computational studies also reveal that LCO affects the slip mode of dislocation and deformation behaviors [3, 40].

### *3.3. Nanoscale heterogeneities due to LCO*

To better understand the softening effect induced by LCO in CuNiCoFe HEAs, generalized stacking fault energies (GSFE) of RSS and LCO models were calculated using a rigid displacement method in molecular statics (see supplementary note 1). For better understanding the spatial variation of LCO creating nanoscale heterogeneities as illustrated in previous studies [5, 9], both local SFEs and local unstable stacking fault energies (USFE) were plotted in figure 4 (see supplementary note 1). Figures 4(a) and (c) show the probability density distributions of Local SFEs and local USFEs, respectively, which follow a Gaussian profile. The average SFEs of LCO samples are about 28 mJ $m^{-2}$, slightly higher than that of RSS (25 mJ $m^{-2}$). Additionally,

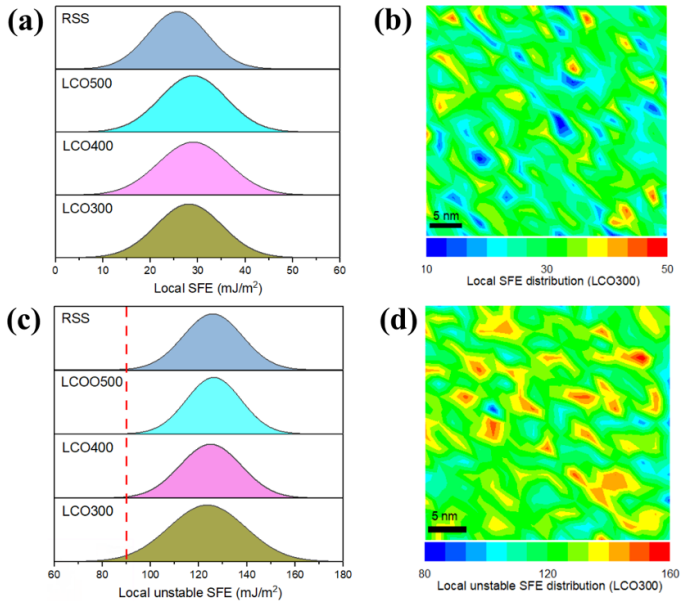


**Figure 4.** Statistical distributions of local properties. Probability density distributions of both (a) local stacking fault energy (SFE) and (c) local unstable SFE for random solid solution (RSS) and LCO samples. Spatial distribution of complex (b) local SFE and (d) local unstable SFE in LCO300.

the average USFEs of LCO300 is 123 mJ $m^{-2}$, smaller than that of RSS (125 mJ $m^{-2}$). The significance of USFE ($\gamma_{USF}$) on microstructure evolution and mechanical performance has been extensively studied in previous works [41, 42]. $\gamma_{USF}$ typically corresponds to the energy barrier of the dislocation nucleation event in single crystals during tension. Although the difference of the average $\gamma_{USF}$ of RSS and LCO samples can be neglected. It important to note that due to the spatial distribution of Cu clusters (see figure S2), the local USFEs of some regions in LCO300 is smaller than 90 mJ $m^{-2}$ compared with other samples. As seen in figures 3(b) and (d), the local SFEs and local USFEs are highly heterogeneous over space, with nanoscale domains showing much different material properties. For example, the experimental work conducted by Smith *et al* [43] revealed that a greater variation in separation distances of extended dislocation was observed in the CoNiCrFeMn HEA due to the highly heterogenous SFEs.

In order to better understand the spatial heterogeneity resulting from Cu clustering, a series of $Cu_x(NiCoFe)_{1-x}$ ($x = 0.1, 0.15, \ldots 0.9$) HEA RSS models were used to describe the spatial distribution of Cu in the LCO models. Note that when $x$ is equal to 0.25, the model agrees with the equiatomic RSS CuNiCoFe model. The GSFEs of these models were then calculated and compared, in figure 5(a). The results indicate that when the Cu fraction exceeds 60% or falls below 35%, the $\gamma_{USF}$ decreases rapidly, indicating the important role of Cu in tailoring GSFEs. When $x$ is equal to 0.9, the difference of $\gamma_{USF}$ is 14 mJ $m^{-2}$ compared to the RSS model ($x = 0.25$), revealing that it is easier to nucleate dislocations in Cu-rich regions. Additionally, the GSFEs of pure Cu, random NiCoFe sample and CuNiCoFe HEA sample are calculated in figure 5(b). Comparing their $\gamma_{USF}$ demonstrates that the dislocations are easier to nucleated from the Cu-rich regions. To confirm the conclusion, the process of dislocation nucleation in the LCO300 model was plotted. As shown in figures 5(c)–(e), partial dislocations (PDs), represented by the green lines, nucleate from Cu-rich regions and slip to Cu-depleted regions.

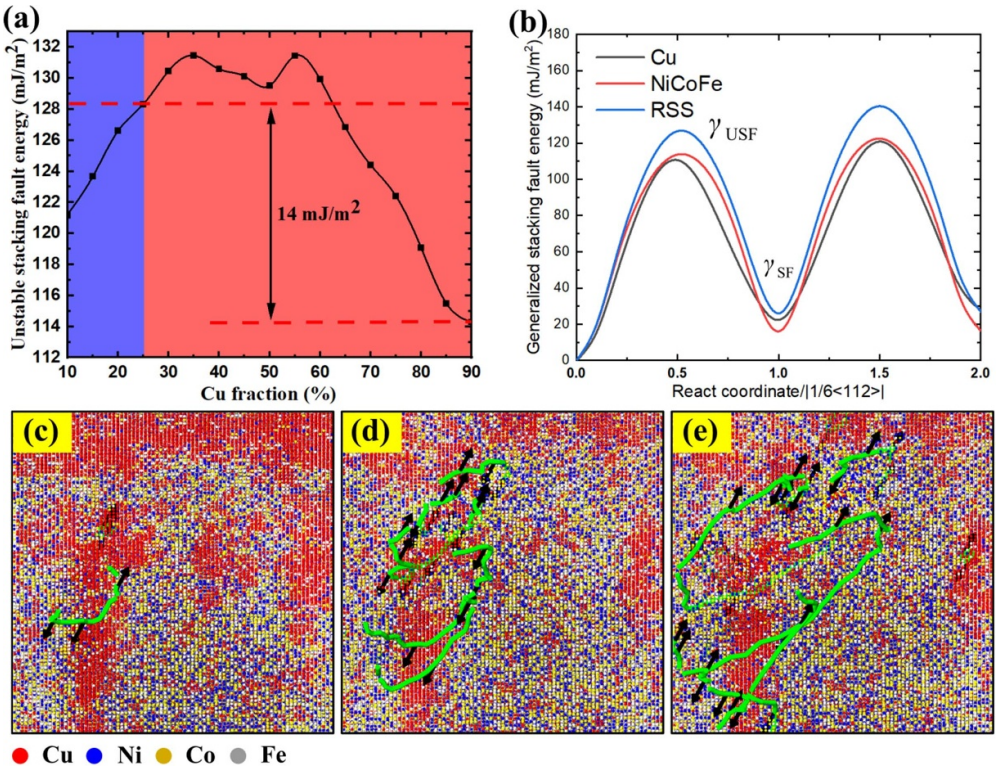


**Figure 5.** Impact of concentration inhomogeneity on generalized stacking fault energies and nucleation of dislocations in LCO samples. (a) $\gamma_{USF}$ of $Cu_x(NiCoFe)_{1-x}$ HEA with x from 0.1 to 0.9. (b) Generalized stacking fault energy for pure Cu, random NiCoFe sample and CuNiCoFe HEA sample. (c)–(e) Dislocation nucleation from the Cu-rich regions and propagation into other regions. Green lines represent the Shockley partial dislocation and the dark arrow denotes the Burgers vector.

The $\gamma_{USF}$ of the Cu-depleted model is also smaller than that of the RSS model as shown in figure 5(b), resulting in the softening of ultimate strength in LCO models.

Besides, an interesting phenomenon concerning the FCC–body-centered cubic (BCC) phase transformation was also observed. According to previous studies [44], the FCC–BCC–HCP phase transformation occurs at high strain rate, and the BCC phase serves as the high-energy transition phase during deformation. A lower strain rate of $1 \times 10^7$ $s^{-1}$ was tested but the FCC–BCC–HCP phase transformation was also observed. The FCC phases transform to BCC phases following the Bain path [45], in which the FCC lattice is sheared by half the Burgers vector of a Shockley dislocation and subjected to the tension-compression of Bain type, resulting in the release of local high energy. However, the FCC–BCC phase transformation is homogenous in the RSS model, while it is not the case in the LCO300 model, as shown in the circles in figures 6(b) and (c). In Cu-rich regions, FCC–BCC transformation rarely occurs. To understand the underlying mechanism, the average elemental compositions of the BCC phase in both RSS and LCO models at the strain of 0.062 have been extracted. The result shows that Fe accounts for 32%, which is about 10% higher than the other three elements. Since Fe is the only element that forms a BCC phase of the four elements, it prefers to transform into the BCC phase. Actually, the concentration inhomogeneity induced by LCO

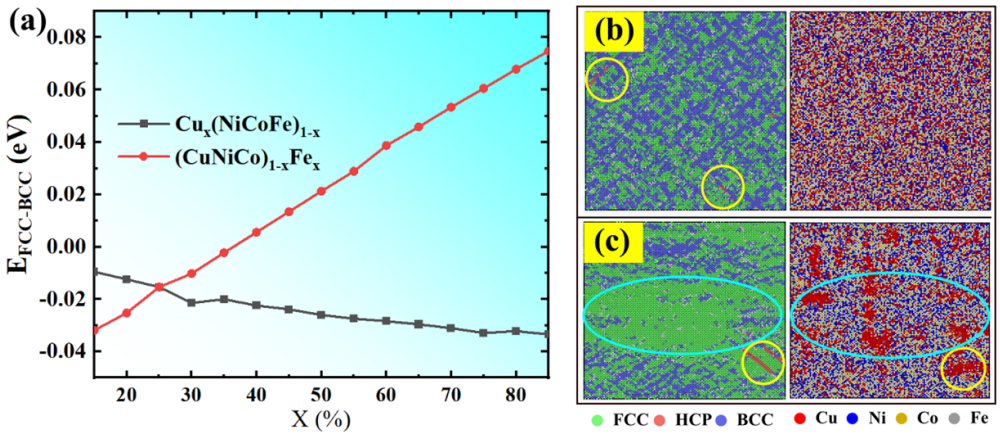


**Figure 6.** (a) Phase stability ($\Delta E_{\mathrm{FCC\,-\,BCC}} = E_{\mathrm{FCC}} - E_{\mathrm{BCC}}$) as a function of chemical compositions estimated by a series of $Cu_x(NiCoFe)_{1-x}$ and $(Cu_xNiCo)_{1-x}Fe_x$ ($x$ = 0.1, 0.15, …0.9) models. Phase transformation from FCC–BCC in (b) RSS and (c) SRO samples during tension. The yellow circles suggest that dislocations are easier to nucleate from within the Cu clusters, and blue circles indicate that FCC–BCC transformation rarely occurs in Cu-rich regions.

usually leads to composite-like microstructures, consisting of different clusters such as FCC-preferred (FCCP) or BCC-preferred (BCCP) clusters. In the present study, the local phase stability (i.e. $\Delta E_{\mathrm{FCC\,-\,BCC}} = E_{\mathrm{FCC}} - E_{\mathrm{BCC}}$) was estimated by a series of $Cu_x(NiCoFe)_{1-x}$ and $(Cu_xNiCo)_{1-x}Fe_x$ ($x = 0.1, 0.15, \ldots 0.9$) models. A positive value of $\Delta E_{\mathrm{FCC\,-\,BCC}}$ means that the BCC phase is more stable while a negative one indicates the opposite. As shown in figure 6(a), value of $\Delta E_{\mathrm{FCC\,-\,BCC}}$ increases proportionally with the Fe fraction. In Cu-rich and Fe-depleted regions, the FCC phase is more stable, which explains the inhomogeneous FCC–BCC phase transformation in the LCO models. Actually, the element-related deformation behaviors have been observed in previous studies [46]. For example, the fraction of Mn near the SF was found to be 30% higher than that in the FCC matrix in the dual-phase $Cr_{20}Mn_6Fe_{34}Co_{34}Ni_6$ HEA [46]. Accordingly, the concentration inhomogeneity may tailor the deformation behaviors in very complex manners, especially in HEAs with atomic segregations and LCO.

## 4. Conclusion

In this paper, the impact of LCO on the ultimate strength and deformation behaviors in the CuNiCoFe HEA was investigated using MD. The chemical affinity and exclusivity drive atomic segregation and the formation of LCO. The CuNiCoFe HEA decompose by Cu clusters since the configuration entropy is insufficient to compete against the mixing enthalpy as the annealing temperature decreases. The result shows that LCO induces softening in ultimate strength during tension because of the lower $\gamma_{\mathrm{USF}}$ in the Cu-rich regions. The concentration inhomogeneity induced by LCO lead to composite-like microstructures. The inhomogeneous FCC–BCC transformation in the LCO models confirm this viewpoint. Besides, the decrease of potential energy caused by the formation of LCO leads to an increase of the energy barrier for phase transformation, thus promoting dislocation slips in LCO models. Accordingly, concentration inhomogeneity, including atomic segregation and LCO, profoundly impacts the

deformation behaviors. Moreover, the impact of grain boundary segregation on mechanical properties will be studied in future.

## Data availability statement

All data that support the findings of this study are included within the article (and any supplementary files).

## Acknowledgments

This work was supported by the National Natural Science Foundation of China (Grant Nos. 11872321 and 12192214).

## Conflict of interest

I would like to declare on behalf of my co-authors that the work described is original research and no conflict of interest exists in the submission of this manuscript.

## ORCID iDs

Siyao Shuang https://orcid.org/0000-0002-7457-9735
Xu Zhang https://orcid.org/0000-0001-8481-0059

## References

[1] Zhang W and Zhang Y 2018 Science and technology in high-entropy alloys *Sci. China Earth Sci.* **61** 2
[2] Otto F, Dlouhý A, Pradeep K G, Kuběnová M, Raabe D, Eggeler G and George E P 2016 Decomposition of the single-phase high-entropy alloy CrMnFeCoNi after prolonged anneals at intermediate temperatures *Acta Mater.* **112** 40
[3] Zhang R, Zhao S, Ding J, Chong Y, Jia T, Ophus C, Asta M, Ritchie R O and Minor A M 2020 Short-range order and its impact on the CrCoNi medium-entropy alloy *Nature* **581** 283
[4] Yang X, Xi Y, He C, Chen H, Zhang X and Tu S 2022 Chemical short-range order strengthening mechanism in CoCrNi medium-entropy alloy under nanoindentation *Scr. Mater.* **209** 114364
[5] Ding J, Yu Q, Asta M and Ritchie R O 2018 Tunable stacking fault energies by tailoring local chemical order in CrCoNi medium-entropy alloys *Proc. Natl Acad. Sci.* **115** 8919
[6] Zhang F X *et al* 2017 Local structure and short-range order in a NiCoCr solid solution alloy *Phys. Rev. Lett.* **118** 205501
[7] Li X-G, Chen C, Zheng H, Zuo Y and Ong S P 2020 Complex strengthening mechanisms in the NbMoTaW multi-principal element alloy *npj Comput. Mater.* **6** 70
[8] Wang J, Jiang P, Yuan F and Wu X 2022 Chemical medium-range order in a medium-entropy alloy *Nat. Commun.* **13** 1021
[9] Li Q-J, Sheng H and Ma E 2019 Strengthening in multi-principal element alloys with local-chemical-order roughened dislocation pathways *Nat. Commun.* **10** 3563
[10] Ding Q *et al* 2019 Tuning element distribution, structure and properties by composition in high-entropy alloys *Nature* **574** 223
[11] Chen X *et al* 2021 Direct observation of chemical short-range order in a medium-entropy alloy *Nature* **592** 712
[12] Yin S, Zuo Y, Abu-Odeh A, Zheng H, Li X G, Ding J, Ong S P, Asta M and Ritchie R O 2021 Atomistic simulations of dislocation mobility in refractory high-entropy alloys and the effect of chemical short-range order *Nat. Commun.* **12** 4873

[13] Chen S, Aitken Z H, Pattamatta S, Wu Z, Yu Z G, Srolovitz D J, Liaw P K and Zhang Y W 2021 Simultaneously enhancing the ultimate strength and ductility of high-entropy alloys via short-range ordering *Nat. Commun.* **12** 4953
[14] Koch L, Granberg F, Brink T, Utt D, Albe K, Djurabekova F and Nordlund K 2017 Local segregation versus irradiation effects in high-entropy alloys: steady-state conditions in a driven system *J. Appl. Phys.* **122** 105106
[15] Tanimoto H, Hozumi R and Kawamura M 2022 Electrical resistivity and short-range order in rapid-quenched CrMnFeCoNi high-entropy alloy *J. Alloys Compd.* **896** 163059
[16] Guo S, Chen H and Wang M 2021 Research on the dislocation differences of CoCrFeMnNi with different local chemical orders during room temperature tensile test *J. Alloys Compd.* **868** 159215
[17] Jian W-R, Xie Z, Xu S, Su Y, Yao X and Beyerlein I J 2020 Effects of lattice distortion and chemical short-range order on the mechanisms of deformation in medium entropy alloy CoCrNi *Acta Mater.* **199** 352
[18] Chen S, Aitken Z H, Pattamatta S, Wu Z, Yu Z G, Banerjee R, Srolovitz D J, Liaw P K and Zhang Y-W 2021 Chemical-affinity disparity and exclusivity drive atomic segregation, short-range ordering, and cluster formation in high-entropy alloys *Acta Mater.* **206** 116638
[19] Utt D, Stukowski A and Albe K 2020 Grain boundary structure and mobility in high-entropy alloys: a comparative molecular dynamics study on a $\Sigma 11$ symmetrical tilt grain boundary in face-centered cubic CuNiCoFe *Acta Mater.* **186** 11
[20] Rahul M R, Samal S, Marshal A, Balaji V I N, Pradeep K G and Phanikumar G 2020 Nano-sized Cu clusters in deeply undercooled CoCuFeNiTa high entropy alloy *Scr. Mater.* **177** 58
[21] Verma A, Tarate P, Abhyankar A C, Mohape M R, Gowtam D S, Deshmukh V P and Shanmugasundaram T 2019 High temperature wear in CoCrFeNiCux high entropy alloys: the role of Cu *Scr. Mater.* **161** 28
[22] Lin C-M and Tsai H-L 2010 Equilibrium phase of high-entropy $FeCoNiCrCu_{0.5}$ alloy at elevated temperature *J. Alloys Compd.* **489** 30
[23] Zhou X W, Johnson R A and Wadley H N G 2004 Misfit-energy-increasing dislocations in vapor-deposited CoFe/NiFe multilayers *Phys. Rev.* B **69** 144113
[24] Pan Z and Rupert T J 2017 Formation of ordered and disordered interfacial films in immiscible metal alloys *Scr. Mater.* **130** 91
[25] Sadigh B, Erhart P, Stukowski A, Caro A, Martinez E and Zepeda-Ruiz L 2010 A scalable parallel Monte Carlo algorithm for atomistic simulations of precipitation in alloys *Phys. Rev.* B **85** 184203
[26] Plimpton S 1995 Fast parallel algorithms for short-range molecular dynamics *J. Comput. Phys.* **117** 1
[27] Brink T, Koch L and Albe K 2016 Structural origins of the boson peak in metals: from high-entropy alloys to metallic glasses *Phys. Rev.* B **94** 224203
[28] Tsuzuki H, Branicio P S and Rino J P 2007 Structural characterization of deformed crystals by analysis of common atomic neighborhood *Comput. Phys. Commun.* **177** 518
[29] Stukowski A and Albe K 2010 Extracting dislocations and non-dislocation crystal defects from atomistic simulation data *Modelling Simul. Mater. Sci. Eng.* **18** 085001
[30] Stukowski A 2009 Visualization and analysis of atomistic simulation data with OVITO–the open visualization tool *Modelling Simul. Mater. Sci. Eng.* **18** 015012
[31] Otto F, Yang Y, Bei H and George E P 2013 Relative effects of enthalpy and entropy on the phase stability of equiatomic high-entropy alloys *Acta Mater.* **61** 2628
[32] Cai W, He J, Wang L, Yang W, Xu X, Yaqoob K, Wang Z and Song M 2023 Characterization of chemical short-range order in VCoNi medium-entropy alloy processed by spark plasma sintering *Scr. Mater.* **231** 115463
[33] Li L, Chen Z, Kuroiwa S, Ito M, Yuge K, Kishida K, Tanimoto H, Yu Y, Inui H and George E P 2023 Evolution of short-range order and its effects on the plastic deformation behavior of single crystals of the equiatomic Cr-Co-Ni medium-entropy alloy *Acta Mater.* **243** 118537
[34] MacDonald B E, Fu Z, Wang X, Li Z, Chen W, Zhou Y, Raabe D, Schoenung J, Hahn H and Lavernia E J 2019 Influence of phase decomposition on mechanical behavior of an equiatomic CoCuFeMnNi high entropy alloy *Acta Mater.* **181** 25
[35] Sonkusare R, Divya Janani P, Gurao N P, Sarkar S, Sen S, Pradeep K G and Biswas K 2018 Phase equilibria in equiatomic CoCuFeMnNi high entropy alloy *Mater. Chem. Phys.* **210** 269

[36] Agarwal R, Sonkusare R, Jha S R, Gurao N P, Biswas K and Nayan N 2018 Understanding the deformation behavior of CoCuFeMnNi high entropy alloy by investigating mechanical properties of binary ternary and quaternary alloy subsets *Mater. Des.* **157** 539
[37] Yu P, Du J-P, Shinzato S, Meng F-S and Ogata S 2022 Theory of history-dependent multi-layer generalized stacking fault energy—A modeling of the micro-substructure evolution kinetics in chemically ordered medium-entropy alloys *Acta Mater.* **224** 117504
[38] Gludovatz B, Hohenwarter A, Catoor D, Chang E, George E and Ritchie R 2014 A fracture-resistant high-entropy alloy for cryogenic applications *Science* **345** 1153
[39] Niu C, LaRosa C R, Miao J, Mills M J and Ghazisaeidi M 2018 Magnetically-driven phase transformation strengthening in high entropy alloys *Nat. Commun.* **9** 1363
[40] Cao P 2022 Maximum strength and dislocation patterning in multi–principal element alloys *Sci. Adv.* **8** eabq7433
[41] Li J and Kirchlechner C 2020 Does the stacking fault energy affect dislocation multiplication? *Mater. Charact.* **161** 110136
[42] Rohatgi A, Vecchio K S and Gray G T 2001 The influence of stacking fault energy on the mechanical behavior of Cu and Cu-Al alloys: deformation twinning, work hardening, and dynamic recovery *Metall. Mater. Trans.* A **32** 135
[43] Smith T M, Hooshmand M S, Esser B D, Otto F, McComb D W, George E P, Ghazisaeidi M and Mills M J 2016 Atomic-scale characterization and modeling of 60° dislocations in a high-entropy alloy *Acta Mater.* **110** 352
[44] Xie H, Yin F, Yu T, Lu G and Zhang Y 2015 A new strain-rate-induced deformation mechanism of Cu nanowire: transition from dislocation nucleation to phase transformation *Acta Mater.* **85** 191
[45] Bowles J S and Wayman C M 1972 The bain strain, lattice correspondences, and deformations related to martensitic transformations *Metall. Trans.* **3** 1113
[46] Chen S, Oh H S, Gludovatz B, Kim S J, Park E S, Zhang Z, Ritchie R O and Yu Q 2020 Real-time observations of TRIP-induced ultrahigh strain hardening in a dual-phase CrMnFeCoNi high-entropy alloy *Nat. Commun.* **11** 826